

Enhancement of the Bose glass phase in the presence of an artificial gauge field

Sukla Pal,^{1,2} Rukmani Bai,^{1,3} Soumik Bandyopadhyay,^{1,3} K. Suthar,¹ and D. Angom¹

¹*Physical Research Laboratory, Ahmedabad - 380009, Gujarat, India*

²*Department of Physics, Centre for Quantum Science, and Dodd-Walls Centre for Photonic and Quantum Technologies, University of Otago, Dunedin 9016, New Zealand*

³*Indian Institute of Technology Gandhinagar, Palaj, Gandhinagar - 382355, Gujarat, India*

We examine the effects of an artificial gauge field and finite temperature in a two-dimensional disordered Bose-Hubbard model. The disorder considered is diagonal and quenched in nature. A signature of disorder in the Bose-Hubbard model is the Bose glass phase. Our work shows that the introduction of an artificial gauge field enhances the domain of the Bose glass phase in the phase diagram. Most importantly, the size of the domain can be tuned with the strength of the artificial gauge field. The introduction of the finite temperature effects is essential to relate theoretical results with the experimental realizations. For our studies we use the single site and cluster Gutzwiller mean-field theories. The results from the latter are more reliable as it better describes the correlation effects. Our results show that the Bose glass phase has a larger domain with the latter method.

I. INTRODUCTION

The observation of a superfluid (SF) to Mott insulator (MI) transition in an optical lattice [1] have opened a new paradigm to explore the physics of quantum many-body systems. Optical lattices are clean and highly controllable; in contrast, the condensed matter systems of interest are never devoid of impurities. Thus, some of the fundamental questions in condensed matter physics are related to quantum phase transitions in the presence of disorder. The presence of disorder constrains the evolution of a quantum system in the Hilbert space and gives rise to quantum glassy phases like Bose glass (BG) [2, 3] and phenomena like Anderson localization [4–7]. The early theoretical investigations of disordered Bose Hubbard model (DBHM) [2, 8] showed that there is no MI-SF transition in presence of diagonal disorder as the BG phase always occurs as the intermediate phase. The theorem of inclusion [9, 10] agrees well with this prediction while identifying BG phase as a Griffiths phase containing the rare regions. In these rare-regions, the energy gap of adding another boson to the system vanishes and thus can be identified as SF islands.

The DBHM have been studied with diverse techniques: mean field [11], projected Gutzwiller method [3], site independent and multisite mean-field method [12, 13], stochastic mean field [14], quantum Monte Carlo [15–17], density matrix renormalisation group (DMRG) [18, 19] for 1D system and numerous others [20–24]. In all the cases the introduction of disorder leads to the emergence of BG phase which is characterized by finite compressibility and zero superfluid stiffness. In the present work, we study 2D DBHM at finite temperatures using single site Gutzwiller and cluster Gutzwiller mean field theories. More importantly, we examine the effect of the artificial gauge fields in DBHM. Here, it must be emphasized that most of the theoretical investigations of DBHM are at zero temperatures, but the experimental realizations are at finite temperatures. This gap is addressed in the present work by examining the consequent effects of thermal fluctuations to the BG phase. One key finding is the presence of normal fluid (NF) phase at finite temperatures and melting of Bose glass phase. The latter is consistent with the findings reported in ref. [25].

In optical lattices it is possible to create an equivalent of Lorentz force with artificial gauge fields [26–31] and is associated with what is referred to as synthetic magnetic field. The introduction of the artificial gauge field breaks time reversal symmetry and modify the band structure. Through the introduction of tunable artificial gauge field it has been possible to observe the single particle mobility edge [32] in zig-zag chains. Apart from the transport properties, the localization effect of the artificial gauge field can enhance the glassy features of DBHM. Indeed, our study reveals that localization in DBHM can be controlled through the artificial gauge field. For this we use Edward Anderson order parameter (EAOP) as a measure of localization while tuning the strength of artificial gauge field. The EAOP is a measure of number fluctuation over disorder realizations and it is finite for the BG phase, but zero and close to zero for the MI and SF phases, respectively. From the values of EAOP we find that there is enhancement of the BG phase in the presence of artificial gauge field. From the experimental point of view this is important as it could facilitate detailed studies of the BG phase.

Experimentally, DBHM can be realized by the addition of speckle type of disorder [33–35], or by the generation of incommensurate multichromatic lattice [36, 37]. Indirect measurements on SF-BG transition have been reported in 1D [38] and 3D [39, 40] systems through transport and coherence measurements. In 2D, the observation of center of mass dynamics [41] has been theoretically proposed as a method to detect the BG phase while ref. [42] suggests measuring the radius of the atomic cloud. Replica symmetry breaking [43, 44] also has been proposed as a possible detection scheme. In spite of these various proposals and progresses towards the realization of a Bose glass, a clear and unambiguous experimental evidence of BG phase is yet to be achieved. In future studies, quantum gas microscopes [45] could probe the properties of the BG phase as it can study the SF islands in BG phase. And, recent work has proposed it as an experimental tool to detect BG phases [25].

This paper is organized as follows. In the Section II we give an account of the single site and cluster Gutzwiller mean field theories. This is then followed by a description of the artificial gauge field and observable measures to distinguish

different phases in Section III and IV. Then, in Section V we provide detailed description of the results obtained from our studies and discuss our observations. And, we then conclude in Section VI.

II. MODEL AND GUTZWILLER MEAN FIELD THEORY

The DBHM for a square lattice with nearest neighbour hopping is defined by the Hamiltonian

$$\hat{H} = - \sum_{p,q} \left[J_x \left(\hat{b}_{p+1,q}^\dagger \hat{b}_{p,q} + \text{H.c.} \right) + J_y \left(\hat{b}_{p,q+1}^\dagger \hat{b}_{p,q} + \text{H.c.} \right) \right] + \sum_{p,q} \hat{n}_{p,q} \left[\frac{U}{2} (\hat{n}_{p,q} - 1) - \tilde{\mu}_{p,q} \right], \quad (1)$$

where p (q) is the lattice index along x (y) axis, $\hat{b}_{p,q}^\dagger$ ($\hat{b}_{p,q}$) is the creation (annihilation) operator for a boson at the (p, q) lattice site, and $\hat{n}_{p,q}$ is the boson density operator; J_x (J_y) is the hopping strength between two nearest neighbour sites along x (y) axis, $U > 0$ is the on-site inter-atomic interaction strength, and $\tilde{\mu}_{p,q} = \mu - \epsilon_{p,q}$ is the local chemical potential. The disorder is introduced through the random energy offset $\epsilon_{p,q}$ which are uniformly distributed independent random numbers $r_{p,q} \in [-D, D]$ and D is bound of random numbers. Depending on the ratio of J and U the above Hamiltonian can describe three possible phases of the system — MI, BG and SF [2]. In the strong on-site interaction limit ($J/U \rightarrow 0$) the system is either in the MI phase (gapped phase), or in the BG phase. Whereas the system is in SF phase when the tunneling overcomes repulsive interaction.

A. Zero temperature Gutzwiller mean-field theory

In the present work we employ the Gutzwiller mean-field theory to compute the properties of the DBHM. In this section we describe two variants of the Gutzwiller mean field theory: First is the single site Gutzwiller mean-field (SGMF) method, where the lattice sites are correlated through a scalar mean field ϕ and cannot describe entangled states such as the quantum Hall state. And, the second is the cluster Gutzwiller mean field (CGMF) method, which incorporates the correlation within a cluster of neighbouring lattice sites exactly and inter-cluster correlation through ϕ . A larger cluster captures the correlation effects better but at the cost of higher computation.

1. SGMF method

In the SGMF method, $\hat{b}_{p,q}$ ($\hat{b}_{p,q}^\dagger$) at a particular lattice site (p, q) is decomposed into mean field $\phi_{p,q}$ ($\phi_{p,q}^*$) and fluctuation $\delta\hat{b}_{p,q}$ ($\delta\hat{b}_{p,q}^\dagger$) parts as

$$\hat{b}_{p,q} = \phi_{p,q} + \delta\hat{b}_{p,q}, \quad (2a)$$

$$\hat{b}_{p,q}^\dagger = \phi_{p,q}^* + \delta\hat{b}_{p,q}^\dagger \quad (2b)$$

where, $\phi_{p,q} = \langle \hat{b}_{p,q} \rangle$, and $\phi_{p,q}^* = \langle \hat{b}_{p,q}^\dagger \rangle$ are the mean field and its complex conjugate, respectively. The expectations are defined with respect to the ground state of the system. Employing this decomposition, the Hamiltonian in Eq. (1) is reduced to the SGMF Hamiltonian

$$\hat{H}^{\text{MF}} = \sum_{p,q} \left\{ -J_x \left[\left(\hat{b}_{p+1,q}^\dagger \phi_{p,q} + \phi_{p+1,q}^* \hat{b}_{p,q} - \phi_{p+1,q}^* \phi_{p,q} \right) + \text{H.c.} \right] - J_y \left[\left(\hat{b}_{p,q+1}^\dagger \phi_{p,q} + \phi_{p,q+1}^* \hat{b}_{p,q} - \phi_{p,q+1}^* \phi_{p,q} \right) + \text{H.c.} \right] + \left[\frac{U}{2} \hat{n}_{p,q} (\hat{n}_{p,q} - 1) - \tilde{\mu}_{p,q} \hat{n}_{p,q} \right] \right\}, \quad (3)$$

where terms up to linear in fluctuation operators are considered and those quadratic in fluctuation operators are neglected. The total Hamiltonian in the above expression can be rewritten as $\hat{H}^{\text{MF}} = \sum_{p,q} \hat{H}_{p,q}^{\text{MF}}$, where $\hat{H}_{p,q}^{\text{MF}}$ is the single site mean field Hamiltonian. The mean field $\phi_{p,q}$ can be identified as the SF order parameter which defines the MI to BG phase-transition in DBHM. Thus, $\phi_{p,q}$ is zero, when the system is in MI phase, and finite in BG as well as in the SF phase.

To compute the ground state of the system the Hamiltonian matrix of $\hat{H}_{p,q}^{\text{MF}}$ can be diagonalized for each lattice site (p, q) separately. And, then the ground state of the system is direct product of the single site ground states $|\psi\rangle_{p,q}$. Using the Gutzwiller approximation, the ground state of the system is

$$|\Psi_{\text{GW}}\rangle = \prod_{p,q} |\psi\rangle_{p,q} = \prod_{p,q} \sum_{n=0}^{N_b} c_n^{(p,q)} |n\rangle_{p,q}, \quad (4)$$

where N_b is the maximum allowed occupation number basis (Fock space basis), and $c_n^{(p,q)}$ are the coefficients of the occupation number state $|n\rangle$ at the lattice site (p, q) . From $|\Psi_{\text{GW}}\rangle$ we can calculate $\phi_{p,q}$, the SF order parameter, as

$$\phi_{p,q} = \langle \Psi_{\text{GW}} | \hat{b}_{p,q} | \Psi_{\text{GW}} \rangle = \sum_{n=0}^{N_b} \sqrt{n} c_{n-1}^{(p,q)*} c_n^{(p,q)}. \quad (5)$$

From the above expression it is evident that $\phi_{p,q}$ is zero in the MI phase as only one occupation number state $|n\rangle$ contributes to $|\psi\rangle_{p,q}$ and hence only one $c_n^{(p,q)}$ has nonzero value. Similarly, the occupancy and number fluctuation at a lattice site are

$$\langle \hat{n}_{p,q} \rangle = \sum_{n=0}^{N_b} |c_n^{(p,q)}|^2 n_{p,q}, \quad (6)$$

$$\delta n_{p,q} = \sqrt{\langle \hat{n}_{p,q}^2 \rangle - \langle \hat{n}_{p,q} \rangle^2} \quad (7)$$

In the MI phase $\delta n_{p,q}$ is zero, which makes MI phase incoherent. In the BG and SF phase $\delta n_{p,q}$ has nonzero value, but the value of $\delta n_{p,q}$ in the BG phase is very small which arises due to the presence of SF islands in the BG phase. The nonzero and relatively large $\delta n_{p,q}$ in the SF phase indicates strong phase coherence. Thus $\delta n_{p,q}$ can also be considered as the order parameter for MI-BG phase transition.

2. CGMF method

In the CGMF method, to incorporate the hopping term exactly and hence improve the correlation effects, the total lattice considered is partitioned into clusters. That is, for an optical lattice of dimension $K \times L$, we can separate it into W clusters (C) of size $M \times N$, that is $W = (K \times L)/(M \times N)$. Thus, the case of CGMF with $M = N = 1$ is equivalent to SGMF. In CGMF, the kinetic energy or the hopping term is decomposed into two types. First is the intra-cluster or hopping within the lattice sites in a cluster, and second is the inter-cluster which is between neighbouring lattice sites which lie on the boundary of different clusters. The details of the present implementation of the CGMF method is reported in ref. [46] and the Hamiltonian of a single cluster is

$$\begin{aligned} \hat{H}_C = & - \sum_{p,q \in C} ' \left[J_x \hat{b}_{p+1,q}^\dagger \hat{b}_{p,q} + J_y \hat{b}_{p,q+1}^\dagger \hat{b}_{p,q} + \text{H.c.} \right] \\ & - \sum_{p,q \in \delta C} \left[J_x (\phi_{p+1,q}^c)^* \hat{b}_{p,q} + J_y (\phi_{p,q+1}^c)^* \hat{b}_{p,q} + \text{H.c.} \right] \\ & + \sum_{p,q \in C} \left[\frac{U}{2} \hat{n}_{p,q} (\hat{n}_{p,q} - 1) - \tilde{\mu}_{p,q} \hat{n}_{p,q} \right] \end{aligned} \quad (8)$$

where $(\phi_{p,q}^c)^* = \sum_{p',q' \notin C} \langle \hat{b}_{p',q'} \rangle$ is the SF order parameter at the lattice site (p, q) which lies at the boundary of neighbouring cluster. The prime in the summation of the first term is to indicate that the $(p+1, q)$ and $(p, q+1)$ lattice points are also within the cluster. And, in the second term δC denotes the lattice sites at the boundary of the cluster. The matrix element of \hat{H}_C is defined in terms of the cluster basis states

$$|\Phi_c\rangle_\ell = \prod_{q=0}^{N-1} \prod_{p=0}^{M-1} |n_p^q\rangle, \quad (9)$$

where $|n_p^q\rangle$ is the occupation number basis at the (p, q) lattice site, and $\ell \equiv \{n_0^0, n_1^0, \dots, n_{M-1}^0, n_0^1, n_1^1, \dots, n_{M-1}^1, \dots, n_{M-1}^{N-1}\}$ is the index quantum number to identify the cluster state. After diagonalizing the Hamiltonian, we can get the ground state of the cluster as

$$|\Psi_c\rangle = \sum_{\ell} C_{\ell} |\Phi_c\rangle_{\ell}. \quad (10)$$

where C_{ℓ} is the coefficient of the cluster state. The ground state of the entire $K \times L$ lattice, like in SGMF, is the direct product of the cluster ground states

$$|\Psi_{\text{GW}}^c\rangle = \prod_k |\Psi_c\rangle_k \quad (11)$$

where, k is the cluster index and varies from 1 to W . The SF order parameter ϕ is computed similar to Eq. (5) as

$$\phi_{p,q} = \langle \Psi_{\text{GW}}^c | \hat{b}_{p,q} | \Psi_{\text{GW}}^c \rangle. \quad (12)$$

With respect to cluster basis, the average occupancy and number fluctuation of lattice sites in the k th cluster are

$$\langle \hat{n} \rangle_k = \frac{\sum_{p,q \in C} \langle \hat{n}_{p,q} \rangle_k}{MN} \quad (13)$$

$$(\delta n)_k = \sqrt{\langle \hat{n}^2 \rangle_k - \langle \hat{n} \rangle_k^2}. \quad (14)$$

For the entire lattice, the average density can be defined as the mean of the average occupancy of the clusters.

B. Finite temperature Gutzwiller mean field theory

To incorporate finite temperature effects we require the entire set of eigenvalues and eigenfunctions obtained from the diagonalization of the mean field Hamiltonian. So, in the case of SGMF we use all the single site eigenvectors $|\psi\rangle_{p,q}^l$ and corresponding eigenvalues $E_{p,q}^l$ to define the single site partition function

$$Z = \sum_{l=1}^{N_b} e^{-\beta E_l}, \quad (15)$$

where $\beta = 1/k_B T$, T being the temperature of the system. Since the energy E_l is scaled with respect to U , T is in units of U/k_B or in other words in the rest of the paper temperature is defined in terms of the dimensionless unit $k_B T/U$. In a similar way, for the CGMF we can define the cluster partition function in terms of the eigenfunctions $|\Psi_c\rangle_k^l$ and the corresponding eigenvalues. Using the above description, the thermal average of the SF order parameter at the (p, q) lattice site is

$$\langle \phi_{p,q} \rangle = \frac{1}{Z} \sum_l \langle \Psi_c | \hat{b}_{p,q} e^{-\beta E_l} | \Psi_c \rangle_k^l, \quad (16)$$

where $\langle \dots \rangle$ is used to represent thermal averaging and $|\Psi_c\rangle_k^l$ is the l th excited state of the k th cluster within which the (p, q) lattice site lies. Similarly, the occupancy or the density can be computed as

$$\langle \langle \hat{n}_{p,q} \rangle \rangle = \frac{1}{Z} \sum_l \langle \Psi_c | \hat{n}_{p,q} e^{-\beta E_l} | \Psi_c \rangle_k^l, \quad (17)$$

where, following the notations in Eq. (6) and (13), the additional $\langle \dots \rangle$ represents thermal averaging. Once we obtain $\langle \langle \hat{n}_{p,q} \rangle \rangle$, the average density or occupancy is $\langle \rho \rangle = \langle n \rangle = \sum_{p,q} \langle \langle \hat{n}_{p,q} \rangle \rangle / (K \times L)$. Then, like defined earlier, the number fluctuation is

$$\delta n_{p,q} = \sqrt{\langle \langle \hat{n}_{p,q}^2 \rangle \rangle - \langle \langle \hat{n}_{p,q} \rangle \rangle^2}. \quad (18)$$

A new feature of considering finite temperature effects is, it is possible to have vanishing $\langle \phi_{p,q} \rangle$ but with non-integer $\langle \langle \hat{n}_{p,q} \rangle \rangle$. This heralds a new phase in the phase diagram and is referred to as the normal fluid (NF). Thus, at finite temperatures SF order parameter can act as the order parameter for the NF-BG transition. Compared to the NF phase, the MI on the other hand has vanishing $\langle \phi_{p,q} \rangle$ and integer $\langle \langle \hat{n}_{p,q} \rangle \rangle$. So, with vanishing $\langle \phi_{p,q} \rangle$ the change from integer value to non-integer $\langle \langle \hat{n}_{p,q} \rangle \rangle$ can be identified as MI-NF transition.

III. ARTIFICIAL GAUGE FIELD

Artificial gauge fields [26–28] engineered through optical fields can create synthetic magnetic fields for charge neutral ultracold atoms in optical lattices. This generates an equivalent of Lorentz force for these atoms, and optical lattice is, then, endowed with properties analogous to the quantum Hall system. Such a system is an excellent model system to study the physics of strongly correlated states like quantum Hall states and their properties. The same logic also applies to the DBHM. In the Hamiltonian description, the presence of an artificial gauge field induces a complex hopping parameter $J \rightarrow J \exp(i\Phi)$ and accordingly the SGMF Hamiltonian in Eq. (3) is modified to

$$\hat{H}^{\text{MF}} = \sum_{p,q} \left\{ -J_x e^{i\Phi} \left[\left(\hat{b}_{p+1,q}^\dagger \phi_{p,q} + \phi_{p+1,q}^* \hat{b}_{p,q} - \phi_{p+1,q}^* \phi_{p,q} \right) + \text{H.c.} \right] - J_y \left[\left(\hat{b}_{p,q+1}^\dagger \phi_{p,q} + \phi_{p,q+1}^* \hat{b}_{p,q} - \phi_{p,q+1}^* \phi_{p,q} \right) + \text{H.c.} \right] + \left[\frac{U}{2} \hat{n}_{p,q} (\hat{n}_{p,q} - 1) - \tilde{\mu}_{p,q} \hat{n}_{p,q} \right] \right\}, \quad (19)$$

where, Φ is the phase an atom acquires when it traverses around a unit cell or plaquette. The artificial gauge field is considered in the Landau gauge and the phase for hopping along x direction arises via the Peierl's substitution [29, 30]. The artificial gauge field, then, creates a staggered synthetic magnetic flux [31] along y direction. The phase can also be defined in terms of the α , the flux quanta per plaquette, through the relation $\Phi = 2\pi\alpha q$, and the flux quanta is restricted in the domain $0 \leq \alpha \leq 1/2$. In the present work, we examine the properties of bosons in presence of artificial gauge field while experiencing a random local chemical potential. Although, the effect of an artificial gauge field on BHM is quite well studied, the same is not true of DBHM.

IV. CHARACTERIZATION OF STATES

Each of the low temperature phases supported by DBHM has special properties and this leads to unique combinations of order parameters as signatures of each phase. The values of these order parameters also determine the phase boundaries. In Table. I, we list the order parameters corresponding to each phase.

A. Superfluid stiffness and compressibility

Phase coherence is a characteristic property of the SF phase, and it is absent in the other phases (MI, NF and BG) supported by DBHM. Thus in the SF phase it requires finite amount of energy to alter the phase coherence, or in other

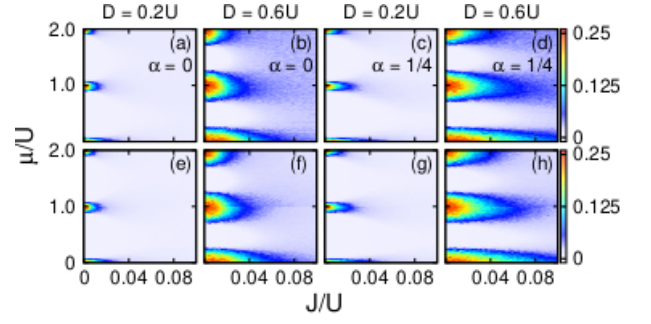


FIG. 1. q_{EA} as a function of μ/U and J/U at zero temperature. (a)-(d) show q_{EA} using SGMF method and (e)-(h) are obtained employing the CGMF method with 2×2 cluster. (c)-(d) show the enhancement of the BG phase region in the presence of an artificial gauge field with $\alpha = 1/4$ compared to (a)-(b) corresponding to $\alpha = 0$ with disorder strengths $D/U = 0.2$ and 0.6 respectively. This enhancement is also captured in (g)-(h) for $\alpha = 1/4$ compared to (e)-(f) using the CGMF method. The increase of BG regions with an increase of D/U is also notable for both in the presence and in the absence of an artificial gauge field. In all the above figures, q_{EA} is obtained by averaging over 50 different disorder distributions.

words, it acquires stiffness towards phase change. This property is referred to as the superfluid stiffness ρ_s , and hence plays an important role in determining the phase boundary between BG and SF phase. To compute ρ_s , a twisted boundary condition (TBC) is imposed on the state. If the TBC is applied along the x direction, the hopping term in the DBHM is transformed as

$$J_x (\hat{b}_{p+1,q}^\dagger \hat{b}_{p,q} + \text{H.c.}) \rightarrow J_x (\hat{b}_{p+1,q}^\dagger \hat{b}_{p,q} e^{i2\pi\varphi/L} + \text{H.c.}), \quad (20)$$

where, φ is the phase shift or twist applied to the periodic boundary condition, L is the size of the lattice along x direction, and $2\pi\varphi/L$ is phase shift of an atom when it hops between nearest neighbours. Accordingly, ρ_s is computed employing the following expression [19]

$$\rho_s = \frac{L}{8\pi^2} \left. \frac{\partial^2 E_0}{\partial \varphi^2} \right|_{\varphi=0}. \quad (21)$$

where E_0 is the ground state energy with TBC. The SF phase is a compressible state as δn is finite. However, MI phase and strongly correlated phase like quantum Hall states are incompressible. Thus, the compressibility κ is a property of the system which can be employed a diagnostic to support the phases determined through the order parameters. By definition, κ is given by

$$\kappa = \frac{\partial \langle \hat{n} \rangle}{\partial \mu}. \quad (22)$$

That is, κ is the sensitivity of n to the change of μ .

B. Edwards-Anderson order parameter

For a disordered system the natural and hence, more appropriate order parameter is the Edwards-Anderson order parameter (EAOP). It can distinguish the Griffiths phase by its non

zero value and can describe the effect of disorder better than other properties like ρ_s , κ , structure factor, etc. In the studies with mean field theory, EAOP was first introduced to detect the non trivial breaking of ergodicity. Since then various type of EAOP have been proposed in literature [43, 44, 47, 48]. In our study we consider the EAOP of the following form [43]

$$q_{\text{EA}} = \overline{\langle \hat{n}_{p,q} \rangle^2} - \overline{\langle \hat{n}_{p,q} \rangle}^2, \quad (23)$$

where, $n_{p,q}$ is the number of atoms at the (p, q) lattice site. The above expression involves two types of averages: $\langle \dots \rangle$ represents thermal; and $\overline{\dots}$ indicates average over disorder distribution. For the $\langle \dots \rangle$ we consider all the excited states. From the definition, as the MI phase is identified by integer values of $\langle \hat{n}_{p,q} \rangle$ q_{EA} is zero. In the SF phase $\langle \hat{n}_{p,q} \rangle$ is real and $\delta n_{p,q}$ is finite, however, for the clean system q_{EA} is zero as $\langle \hat{n}_{p,q} \rangle$ is homogeneous. With disorder, $\langle \hat{n}_{p,q} \rangle$ is inhomogeneous in the SF phase and hence, q_{EA} is finite but small $O(10^{-3})$ [25]. In the BG phase q_{EA} is relatively large due to correlation between number density and disorder. Thus using q_{EA} the BG phase is distinguishable from MI and NF phases in the present in the system. In zero temperature limit we define q_{EA} as

$$q_{\text{EA}}|_{(T=0)} = \overline{\langle \hat{n}_{p,q} \rangle^2} - \overline{\langle \hat{n}_{p,q} \rangle}^2, \quad (24)$$

where we consider expectations only for the ground state.

Quantum phase	Order parameter
Superfluid (SF)	$q_{\text{EA}} > 0, \rho_s > 0, \kappa > 0, \phi \neq 0$
Mott insulator (MI)	$q_{\text{EA}} = 0, \rho_s = 0, \kappa = 0, \phi = 0$
Bose glass (BG)	$q_{\text{EA}} > 0, \rho_s = 0, \kappa > 0, \phi \neq 0$
Normal fluid (NF)	$q_{\text{EA}} > 0, \rho_s = 0, \kappa > 0, \phi = 0$

TABLE I. Classification of quantum phases and the order parameters supported by DBHM at zero and finite temperatures.

V. RESULTS AND DISCUSSIONS

To compute the ground state of the system and determine the phase diagram, we scale the parameters of the DBHM Hamiltonian with respect to the interaction strength U . So, the relevant parameters of the model are J/U , μ/U and D/U . We, then, determine the phase diagram of the DBHM in the $J/U - \mu/U$ plane for different values of D/U , and one unique feature of the model is the emergence of the BG phase. The local glassy nature of the BG phase leads to very different properties from the incompressible and gapped MI phase, and compressible and gapless SF phase. Thus as mentioned earlier, one of the key issues in the study of DBHM is to identify appropriate order parameters to distinguish different phases. And, in particular, to determine the BG phase without ambiguity based on its local properties. To construct the phase diagram, we consider a 12×12 square lattice superimposed with a homogeneous disorder distribution.

In DBHM, depending on the magnitude of D/U , the phase diagrams can be classified into three broad categories. First,

at low disorder strength $D/U \leq 0.1$, BG phase emerge in the phase diagram. Second, at moderate disorder strengths $0.2 \leq D/U \leq 1$, the domain of BG phase is enhanced. This is the most important regime to explore the physics of BG phase. The distinctive features in this range consist of shrinking of MI phase and enhancement of the BG phase. Finally, at very high disorder strengths $D/U > 1$, the MI phase disappears and DBHM supports only two phases, BG and SF. For reference the selected zero temperature results are shown in the Appendix.

A. Zero temperature results

The synthetic magnetic field arising from the introduction of the artificial gauge field localizes the bosons and suppresses their itinerant property. This manifests as a larger MI lobe in the presence of artificial gauge field. However, locally the combined effect of disorder and artificial gauge field favours the formation of SF islands. This synergy, then, creates a larger domain of BG phase in the phase diagram. In terms of identifying the phase boundaries, unlike in the $\alpha = 0$ where ρ_s has linear dependence on J/U in the SF domain, ρ_s cannot be used here as it exhibits no dependence on J/U . The two possible causes of this are: the TBC required to compute ρ_s modifies the magnetic unit cell associated with the chosen value of α ; and with $\alpha \neq 0$ the SF phase contains vortices which reduce the SF phase coherence. So, we use q_{EA} as the order parameter to distinguish BG phase from the MI and SF phases. For consistency we compute q_{EA} both for $\alpha = 0$ and $\alpha = 1/4$ employing SGMF and the results are shown in Fig. 1(a)-(d), where q_{EA} is shown as a function of μ/U and J/U . The general trend is that q_{EA} is zero in MI and $O(10^{-3})$ in the SF phase, and $O(10^{-1})$ in BG phase. From the figure, the presence of the BG phase between different MI lobes is discernible from the finite values of q_{EA} and it is consistent with the phase diagram determined from ρ_s shown in Fig. 6(g)-(j) in Appendix. We can define sharp MI-BG and SF-BG boundaries in the phase diagram by defining a threshold value of q_{EA} between the Mott lobes, however, this is non-trivial for the patina of BG phase present at the tip of Mott lobes. This is the domain where the MI-SF quantum phase transition is driven by phase fluctuations and consequently, the number fluctuation is highly suppressed. As a result the value of q_{EA} is negligible and it cannot be used to distinguish BG and SF phases [12, 14]. Thus, to identify the BG domain it is essential to complement the results from q_{EA} with those of other quantities.

For $\alpha = 1/4$, the region with finite values of q_{EA} increases significantly. This is discernible from the plot of q_{EA} in Fig. 1(d). For the case of $D/U = 0.6$, when $\alpha = 1/4$, the q_{EA} is finite with a value of ≈ 0.2 upto $J/U \approx 0.03$. Whereas, with $\alpha = 0$ as shown in Fig. 1(b), q_{EA} has similar value only upto $J/U \approx 0.02$. This indicates the enhancement of BG region in the presence of the artificial gauge field. Employing CGMF method with 2×2 cluster, the values of the q_{EA} obtained are shown in Fig. 1(e)-(h). One important change is that, q_{EA} is no longer zero in the MI phase, but it is of $O(10^{-6})$.

This is due to the presence of particle-hole excitations in the cluster states. And, the non-zero value of q_{EA} is consistent with the results reported in a previous work [44]. The figures show similar trends of artificial gauge field induced enhancement of the BG region in the phase diagram. The increase of BG regions with the increase of D/U is also notable for both $\alpha = 0$ and $\alpha = 1/4$. Another observation is that, q_{EA} obtained from the CGMF method contains less fluctuations and thus describes the boundary of SF-BG transition better compared to the SGMF method. Increasing the cluster size CGMF can describe the BG-SF boundary more accurately but at the cost of much higher computational resources.

B. Finite temperature results

The important outcome of finite temperature is the emergence of a new phase, the NF phase. This new phase, like the SF phase, has real commensurate number of particles per site. So, the NF phase has some features common to both the MI and SF phases. Previous works reported the appearance of the NF phase at finite temperatures in the case of the canonical Bose-Hubbard model [49], and extended Bose-Hubbard model with nearest neighbour interactions [50, 51].

1. $\alpha = 0$

The effect of the thermal fluctuations to the q_{EA} , in absence of artificial gauge field ($\alpha = 0$), is shown in Fig. 2(g). The results presented in the figure correspond to $D/U = 0.6$ and each plot is an average over 500 realizations of disorder distributions. With increasing temperature there is a monotonic decrease in q_{EA} , which indicates the *melting* of BG phase. Along with the BG phase the MI phase also melts, however, this is not apparent from the values of q_{EA} . And, the extent of melting can be inferred from the phase diagram. To illustrate this point the phase diagram of DBHM at different temperatures are shown in Fig 2(a-f). As mentioned earlier, previous studies have also reported the melting of MI phase due to thermal fluctuations [49]. But a clear theoretical description and phase diagram incorporating finite temperature effects are lacking. Our present work shows that the BG phase also melts due to thermal fluctuations. Here, the key point is the SF islands, which are hallmark of the BG phase, melts into NF. This arises from the local nature of the SF islands in BG phase, which as a result is affected by the local nature of the thermal fluctuations. The bulk SF phase, on the other hand, has long range phase correlations and is more robust against local fluctuations stemming from finite temperatures.

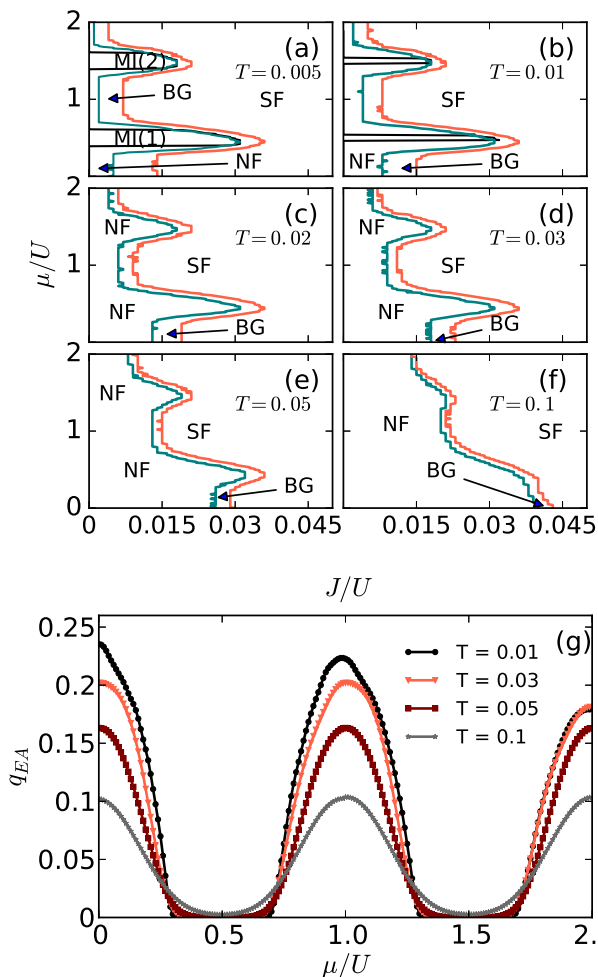


FIG. 2. Finite temperature phase diagram using SGMF method in absence of artificial gauge field for six different temperatures (a) $T = 0.005U/k_B$, (b) $T = 0.01U/k_B$, (c) $T = 0.02U/k_B$, (d) $T = 0.03U/k_B$, (e) $T = 0.05U/k_B$ and (f) $T = 0.1U/k_B$. Disorder strength is fixed at $D = 0.6U$ and each data in the plot is obtained by averaging over 500 different disorder distributions. (g) shows finite temperature effects on Edward-Anderson order parameter (q_{EA}) with $D/U = 0.6$ and J/U being fixed at 0.01. The magnitude of q_{EA} gradually decreases with increase of temperature.

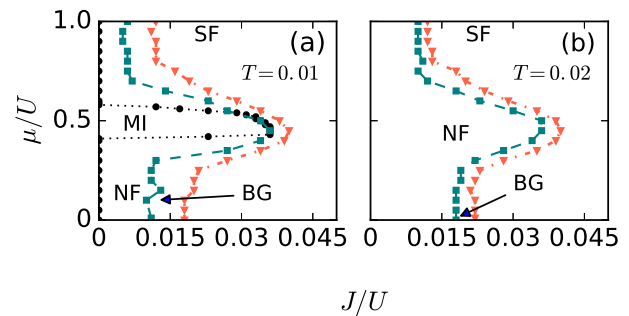


FIG. 3. Finite temperature phase diagram using CGMF for 2×2 cluster in absence of artificial gauge field for two different temperatures (a) $T = 0.01U/k_B$, (b) $T = 0.02U/k_B$; Disorder strength is fixed at $D = 0.6U$ and each data in the plot is obtained by averaging over 50 different disorder distributions.

In the plots the region within the black line is MI phase, whereas, the region bounded by the black and green lines is the NF phase, where ϕ is close to zero $\phi \leq 10^{-6}$. The BG

phase lies in the region bounded by the green and orange lines, and the area right of the orange line is the SF phase. As the temperature is increased, due to the increased thermal fluctuations, the phase diagrams undergo several changes. First, the MI lobes shrink and at $k_B T/U = 0.02$, MI lobes disappear from the phase diagram. This is due to the melting of MI phase and conversion into NF phase. So, as discernible from the comparison of Fig. 2(a) and (b), the MI lobe with $\rho = 1$ is bounded and lies in the domain $0.40 \leq \mu/U \leq 0.6$ at $k_B T/U = 0.005$, but it shrinks to $0.47 \leq \mu/U \leq 0.53$ at $k_B T/U = 0.01$. Second, the region of the BG phase is reduced with increasing temperature. The change is more prominent in the regions which lie between the MI lobes. For example, at $\mu = 0$ the BG phase exists in the domain $0.004 \leq J/U \leq 0.014$ for $k_B T/U = 0.005$. But, it is reduced to $0.008 \leq J/U \leq 0.015$ when the temperature is increased to $k_B T/U = 0.01$. As discernible from Fig. 2(f) at $k_B T/U = 0.1$ the domain is reduced to $0.04 \leq J/U \leq 0.043$. And, third, at finite temperatures the MI lobes are bounded from top and bottom by straight lines in the SGMF results. But, as visible from Fig. 3, the MI boundary is not a straight line with CGMF results. This is on account of the better correlation effects in CGMF, in contrast, SGMF tends to support sharp NF-MI boundaries as a function of μ/U due to short range coupling through ϕ .

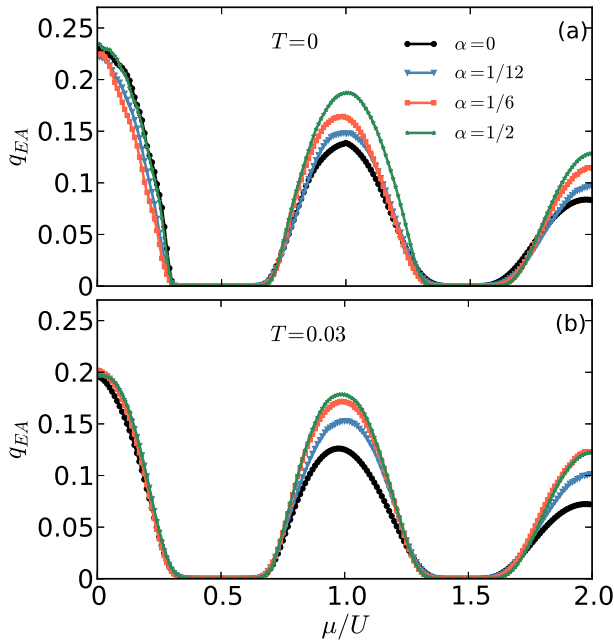


FIG. 4. q_{EA} as a function of μ/U for four different values of α at (a) $T = 0$ (b) $T = 0.03U/k_B$; with fixed disorder strength $D = 0.6U$ and hopping strength $J = 0.02U$. In each subfigure q_{EA} are calculated for $\alpha = 0, 1/12, 1/6$ and $1/2$ and averaged over 500 different disorder distributions.

Based on the above observations of the phase diagrams at different temperatures, the NF-BG and BG-SF phase boundaries shift toward higher J/U with increasing temperature. This is due to higher hopping energy required to prevail over thermal fluctuations. So that the SF phase is present as islands

or homogeneous network in BG and SF phases, respectively. The other important point is that, the SF phase does not melt directly to NF phase. In other words, the BG phase advances into the SF phase with ever decreasing width with increasing temperature. Thus, the BG phase is an intermediate phase between the NF and SF phases. This is the finite temperature equivalent of the zero temperature phase structure, where BG phase is an intermediate phase between the MI and SF phases.

To improve the accuracy of the phase diagram by incorporating additional correlation effects, we compute the phase diagram with CGMF using 2×2 cluster, and the resulting phase diagram is shown in Fig. 3. The results are for the temperatures $k_B T/U = 0.01$ and 0.02 , and for better illustration the phase diagrams of only upto $\mu/U = 1.0$ are shown in the figure. As to be expected the MI lobes are larger in the CGMF results, but the one important change is that the envelope of BG phase around the MI and NF phases is more pronounced. Consequent to the larger MI lobes, the NF and BG phases encompass regions with higher J/U compared with the SGMF results. In particular, at $\mu = 0$ the BG phase occurs in the domain $0.011 \leq J/U \leq 0.018$ and $0.018 \leq J/U \leq 0.022$ for the $k_B T/U = 0.01$ and $k_B T/U = 0.02$, respectively.

2. $\alpha \neq 0$

The thermal fluctuations delocalize the atoms through the entire lattice, and melt MI phase. This tends to reduce ϕ . Whereas, as mentioned earlier, artificial gauge field localizes the atoms, and thereby enhances the MI lobes. So, these two have opposing effects on the DBHM, and the combined effects of these two physical factors on the q_{EA} are shown in Fig. 4. In the figure 4 the plots of q_{EA} for $k_B T/U = 0$ and 0.03 are shown for different α as a function μ/U at $J/U = 0.02$. From the figures it is apparent that the effect of the artificial gauge field is negligible in the region between the $\rho = 0$ and $\rho = 1$ Mott lobes. However, in the regions between other Mott lobes there is an enhancement of the BG phase as indicated by the increase in q_{EA} . As discernible from Fig. 4(a) the value of q_{EA} increases from 0.13 to 0.19 for the region between $\rho = 1$ and $\rho = 2$ corresponding to $0.65 \leq \mu/U \leq 1.36$ for non-zero α at $k_B T/U = 0$. From the figure it is also evident that q_{EA} gradually increases with the increase of α . Consequently, the enhancement of BG phase region in DBHM depends on the strength of artificial gauge field. As a quantitative measure of it, for $\alpha = 0, 1/12, 1/6$ and $1/2$ q_{EA} takes the value 0.139, 0.148, 0.164 and 0.187 respectively around $\mu = U$. To demonstrate the combined effect of finite temperature and artificial gauge field, the phase diagram in terms of q_{EA} is shown in Fig. 5. As the figure is based on 50 disorder realizations, the general trends of q_{EA} observable in Fig. 4 are not apparent. However, from the figure the enlargement of the BG phase region between the MI lobes is discernible. Thus, this implies that the enhancement of the BG phase in presence of artificial gauge field is stable against thermal fluctuations.

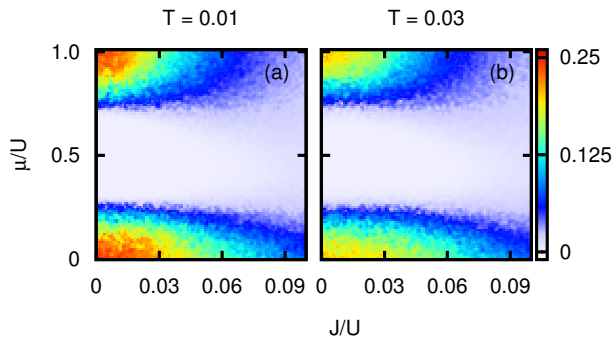


FIG. 5. q_{EA} as a function of μ/U and J/U for $\alpha = 1/4$ for two different values of temperature $T = 0.01U/k_B$ (a) and $T = 0.03U/k_B$. (b) Disorder strength is kept fixed at $D = 0.6U$ and q_{EA} are averaged over 50 different disorder distributions with CGMF method.

VI. CONCLUSIONS

At finite temperatures, the thermal fluctuations lead to melting of the BG phase and formation of NF phase. The emergence of the NF phase at finite temperatures necessitates using a combination of order parameters and properties to identify each phase without ambiguity. More importantly, the BG phase is an intermediate phase between the NF and SF phases. This is similar to the zero temperature phase where the BG phase is an intermediate phase between the MI and SF phases. At higher temperatures the melting of MI phase is complete and only three phases NF, BG and SF phases exist in the system. The addition of artificial gauge field brings about a significant change in the phase diagram by enhancing the BG phase domain, which is observed in the trends of the q_{EA} without any ambiguity. This implies that such enhancements would be observable in quantum gas microscope experiments. To get accurate results with mean field theories it is desirable to use the CGMF theory. It incorporates correlation effects better and the phase diagrams obtained from CGMF are quantitatively different from those obtained from SGMF.

ACKNOWLEDGMENTS

The results presented in the paper are based on the computations using Vikram-100, the 100TFLOP HPC Cluster at Physical Research Laboratory, Ahmedabad, India.

APPENDIX

To determine the MI-BG phase boundary, we consider number fluctuation (δn) as the property which distinguishes the two phases. In the MI phase δn is zero for $D/U = 0$, however, for $D/U \neq 0$, it is non-zero but small due to the disorder. We set $\delta n < 10^{-6}$ as the criterion to identify the MI phase in our computations. On the other hand, to define the BG-SF boundary, we compute the superfluid stiffness (ρ_s).

In BG phase as the SF phase exists as islands the phase coherence is limited to these, so the ρ_s small, and we consider $\rho_s < 10^{-2}$ as the threshold to distinguish the BG from SF phase. In the SF phase as there is phase coherence throughout the system ρ_s is large and it is $O(1)$.

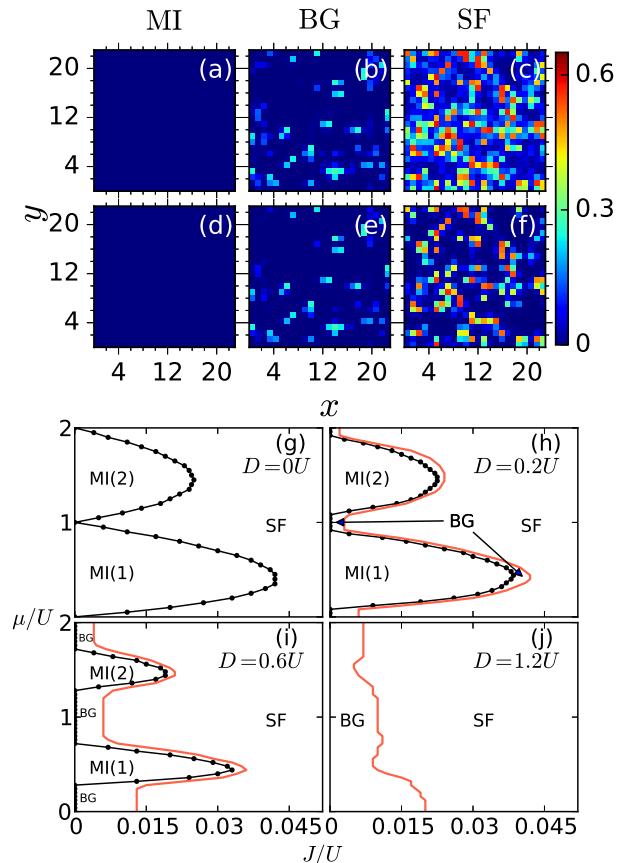


FIG. 6. Order parameter ϕ of DBHM at zero temperature for $J/U = 0.01$ and D/U keeping fixed at 0.6 (a)-(c) without and (d)-(f) with ($\alpha = 1/4$) artificial gauge field. (a) & (d) MI phase with $\mu/U = 0.5$; (b) & (e) BG phase with $\mu/U = 0.1$; and (c) & (f) SF phase with $\mu/U = 1.0$. (g)-(j) equilibrium phase diagram of DBHM using SGMF method at zero temperature in absence of artificial gauge field ($\alpha = 0$) for disorder strengths $D/U = 0, 0.2, 0.6$ and 1.2, respectively for 500 different disorder realizations.

The phase diagrams of DBHM with $\alpha = 0$ at different values of D/U have distinctive features [3]. As examples, the phase diagrams for the case of $D/U = 0, 0.2, 0.6$ and 1.2 obtained from the SGMF method are shown in Fig. 6(g)-(j). With $D/U = 0$, the phase diagram as shown in Fig. 6(g) consists of only two phases MI and SF. With non-zero D/U BG appears in the phase diagram, and as shown in Fig. 6(h) for $D = 0.2$ the domain of the MI phase shrinks and an envelope of BG phase emerges around the MI lobes. From Fig. 6(h), it is clear that the BG phase is most prominent in between the MI lobes. These are the domains with large density fluctuations and small disorder is sufficient to render the bosons itinerant to create islands of SF phase. This, then, leads to the formation of BG phase. When the D/U is increased to

0.6, as shown in Fig. 6(i), the MI lobes shrink further and the area of the BG phase is enlarged. At sufficiently high disorder strength, $D = 1.2U$, the MI phase disappears and phase diagram Fig. 6(j) is composed of only SF and BG phases.

There is an improvement in the phase diagram, which is apparent from the enlarged MI lobes, when the phase diagram is computed using CGMF. In particular, we consider 2×2 cluster and the phase diagrams so obtained are shown in Fig. 7. The overall structure of the phase diagram is qualitatively similar to the SGMF case. However, there are few quantitative changes. For comparison, consider the case of $D/U = 0.6$, based on our results and as visible in Fig. 6(i) and Fig. 7(b), there are three important difference due to better correlation effects encapsulated in the CGMF method. First, the tip of the Mott lobe $\rho = 1$ extends upto 0.035 while it was 0.032 with SGMF. Second, at $\mu/U \simeq 0$, the SF-BG transition occurs at $J/U \approx 0.022$, which in the case of SGMF is at $J/U \approx 0.014$. This is due to the association of BG phase with islands of SF phase, and CGMF captures the phase correlations in these islands better. The SGMF, on the other hand, tends to favour long range phase correlations through the ϕ coupling between

the lattices sites. And, finally, around the tip of the Mott lobes, the area of BG phase increases in CGMF method.

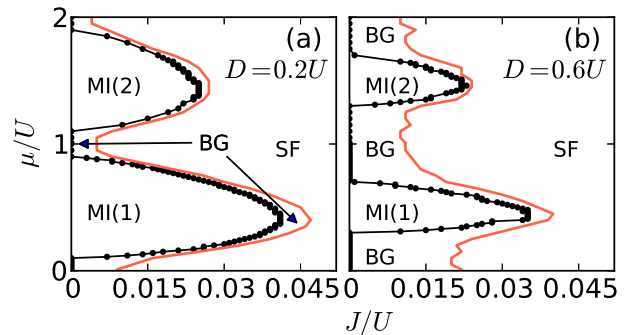


FIG. 7. Equilibrium phase diagram of DBHM using CGMF method with cluster size 2×2 at zero temperature in absence of artificial gauge field for disorder strength (a) $D/U = 0.2$, and (b) $D/U = 0.6$ for 50 different disorder realizations.

-
- [1] M. Greiner, O. Mandel, T. Esslinger, T. W. Hänsch, and I. Bloch, “Quantum phase transition from a superfluid to a Mott insulator in a gas of ultracold atoms,” *Nature (London)* **415**, 39 (2002).
- [2] M. P. A. Fisher, P. B. Weichman, G. Grinstein, and D. S. Fisher, “Boson localization and the superfluid-insulator transition,” *Phys. Rev. B* **40**, 546 (1989).
- [3] C.-H. Lin, R. Sensarma, K. Sengupta, and S. D. Sarma, “Quantum dynamics of disordered bosons in an optical lattice,” *Phys. Rev. B* **86**, 214207 (2012).
- [4] P. W. Anderson, “Absence of diffusion in certain random lattices,” *Phys. Rev.* **109**, 1492 (1958).
- [5] T. Schulte, S. Drenkelforth, J. Kruse, W. Ertmer, J. Arlt, K. Sacha, J. Zakrzewski, and M. Lewenstein, “Routes towards Anderson-like localization of Bose-Einstein condensates in disordered optical lattices,” *Phys. Rev. Lett.* **95**, 170411 (2005).
- [6] J. Billy, V. Josse, Z. Zuo, A. Bernard, B. Hambrecht, P. Lugan, D. Clément, L. Sanchez-Palencia, P. Bouyer, and A. Aspect, “Direct observation of Anderson localization of matter waves in a controlled disorder,” *Nature (London)* **453**, 891 (2008).
- [7] G. Roati, C. D’Errico, L. Fallani, M. Fattori, C. Fort, M. Zaccanti, G. Modugno, M. Modugno, and M. Inguscio, “Anderson localization of a non-interacting Bose-Einstein condensate,” *Nature (London)* **453**, 895 (2008).
- [8] T. Giamarchi and H. J. Schulz, “Anderson localization and interactions in one-dimensional metals,” *Phys. Rev. B* **37**, 325 (1988).
- [9] L. Pollet, N. V. Prokof’ev, B. V. Svistunov, and M. Troyer, “Absence of a direct superfluid to Mott insulator transition in disordered Bose systems,” *Phys. Rev. Lett.* **103**, 140402 (2009).
- [10] V. Gurarie, L. Pollet, N. V. Prokof’ev, B. V. Svistunov, and M. Troyer, “Phase diagram of the disordered Bose-Hubbard model,” *Phys. Rev. B* **80**, 214519 (2009).
- [11] K. V. Krutitsky, A. Pelster, and R. Graham, “Mean-field phase diagram of disordered bosons in a lattice at nonzero temperature,” *New J. Phys.* **8**, 187 (2006).
- [12] P. Buonsante, V. Penna, A. Vezzani, and P. B. Blakie, “Mean-field phase diagram of cold lattice bosons in disordered potentials,” *Phys. Rev. A* **76**, 011602 (2007).
- [13] P. Pisarski, R. M. Jones, and R. J. Gooding, “Application of a multisite mean-field theory to the disordered Bose-Hubbard model,” *Phys. Rev. A* **83**, 053608 (2011).
- [14] U. Bissbort, R. Thomale, and W. Hofstetter, “Stochastic mean-field theory: Method and application to the disordered Bose-Hubbard model at finite temperature and speckle disorder,” *Phys. Rev. A* **81**, 063643 (2010).
- [15] H. Gimpferlein, S. Wessel, J. Schmiedmayer, and L. Santos, “Ultracold atoms in optical lattices with random on-site interactions,” *Phys. Rev. Lett.* **95**, 170401 (2005).
- [16] Ş. G. Söyler, M. Kiselev, N. V. Prokof’ev, and B. V. Svistunov, “Phase diagram of the commensurate two-dimensional disordered Bose-Hubbard model,” *Phys. Rev. Lett.* **107**, 185301 (2011).
- [17] P. Sengupta and S. Haas, “Quantum glass phases in the disordered Bose-Hubbard model,” *Phys. Rev. Lett.* **99**, 050403 (2007).
- [18] S. Rapsch, U. Schollwöck, and W. Zwerger, “Density matrix renormalization group for disordered bosons in one dimension,” *EPL* **46**, 559 (1999).
- [19] M. Gerster, M. Rizzi, F. Tschirsich, P. Silvi, R. Fazio, and S. Montangero, “Superfluid density and quasi-long-range order in the one-dimensional disordered Bose-Hubbard model,” *New J. Phys.* **18**, 015015 (2016).
- [20] R. V. Pai, R. Pandit, H. R. Krishnamurthy, and S. Ramasesha, “One-dimensional disordered bosonic Hubbard model: A density-matrix renormalization group study,” *Phys. Rev. Lett.* **76**, 2937 (1996).
- [21] N. Prokof’ev and B. Svistunov, “Superfluid-insulator transition in commensurate disordered bosonic systems: Large-scale worm algorithm simulations,” *Phys. Rev. Lett.* **92**, 015703 (2004).
- [22] F. Krüger, J. Wu, and P. Phillips, “Anomalous suppression of

- the Bose glass at commensurate fillings in the disordered Bose-Hubbard model,” *Phys. Rev. B* **80**, 094526 (2009).
- [23] F. Krüger, S. Hong, and P. Phillips, “Two distinct Mott-insulator to Bose-glass transitions and breakdown of self-averaging in the disordered Bose-Hubbard model,” *Phys. Rev. B* **84**, 115118 (2011).
- [24] J. Carrasquilla, F. Becca, A. Trombettoni, and M. Fabrizio, “Characterization of the Bose-glass phase in low-dimensional lattices,” *Phys. Rev. B* **81**, 195129 (2010).
- [25] S. J. Thomson, L. S. Walker, T. L. Harte, and G. D. Bruce, “Measuring the Edwards-Anderson order parameter of the Bose glass: A quantum gas microscope approach,” *Phys. Rev. A* **94**, 051601 (2016).
- [26] Y.-J. Lin, R. L. Compton, A. R. Perry, W. D. Phillips, J. V. Porto, and I. B. Spielman, “Bose-Einstein condensate in a uniform light-induced vector potential,” *Phys. Rev. Lett.* **102**, 130401 (2009).
- [27] Y.-J. Lin, R. L. Compton, K. Jiménez-García, W. D. Phillips, J. V. Porto, and I. B. Spielman, “A synthetic electric force acting on neutral atoms,” *Nat. Phys.* **7**, 1745 (2011).
- [28] J. Dalibard, F. Gerbier, G. Juzeliūnas, and P. Öhberg, “Colloquium: Artificial gauge potentials for neutral atoms,” *Rev. Mod. Phys.* **83**, 1523 (2011).
- [29] D. R. Hofstadter, “Energy levels and wave functions of Bloch electrons in rational and irrational magnetic fields,” *Phys. Rev. B* **14**, 2239 (1976).
- [30] K. Jiménez-García, L. J. LeBlanc, R. A. Williams, M. C. Beeler, A. R. Perry, and I. B. Spielman, “Peierls substitution in an engineered lattice potential,” *Phys. Rev. Lett.* **108**, 225303 (2012).
- [31] M. Aidelsburger, M. Atala, S. Nascimbéne, S. Trotzky, Y.-A. Chen, and I. Bloch, “Experimental realization of strong effective magnetic fields in an optical lattice,” *Phys. Rev. Lett.* **107**, 255301 (2011).
- [32] F. A. An, E. J. Meier, and B. Gadway, “Engineering a flux-dependent mobility edge in disordered zigzag chains,” *Phys. Rev. X* **8**, 031045 (2018).
- [33] D. Clément, A. F. Varón, M. Hugbart, J. A. Retter, P. Bouyer, L. Sanchez-Palencia, D. M. Gangardt, G. V. Shlyapnikov, and A. Aspect, “Suppression of transport of an interacting elongated Bose-Einstein condensate in a random potential,” *Phys. Rev. Lett.* **95**, 170409 (2005).
- [34] D. Clément, P. Bouyer, A. Aspect, and L. Sanchez-Palencia, “Density modulations in an elongated Bose-Einstein condensate released from a disordered potential,” *Phys. Rev. A* **77**, 033631 (2008).
- [35] M. White, M. Pasienski, D. McKay, S. Q. Zhou, D. Ceperley, and B. DeMarco, “Strongly interacting bosons in a disordered optical lattice,” *Phys. Rev. Lett.* **102**, 055301 (2009).
- [36] B. Damski, J. Zakrzewski, L. Santos, P. Zoller, and M. Lewenstein, “Atomic Bose and Anderson glasses in optical lattices,” *Phys. Rev. Lett.* **91**, 080403 (2003).
- [37] L. Fallani, J. E. Lye, V. Guarrera, C. Fort, and M. Inguscio, “Ultracold atoms in a disordered crystal of light: Towards a Bose glass,” *Phys. Rev. Lett.* **98**, 130404 (2007).
- [38] B. Gadway, D. Pertot, J. Reeves, M. Vogt, and D. Schneble, “Glassy behavior in a binary atomic mixture,” *Phys. Rev. Lett.* **107**, 145306 (2011).
- [39] M. Pasienski, D. McKay, M. White, and B. DeMarco, “A disordered insulator in an optical lattice,” *Nat. Phys.* **6**, 677 (2010).
- [40] C. Meldgin, U. Ray, P. Russ, D. Chen, D. M. Ceperley, and B. DeMarco, “Probing the Bose glass-superfluid transition using quantum quenches of disorder,” *Nat. Phys.* **12**, 646 (2016).
- [41] M. Yan, H.-Y. Hui, and V. W. Scarola, “Dynamics of disordered states in the Bose-Hubbard model with confinement,” *Phys. Rev. A* **95**, 053624 (2017).
- [42] D. Delande and J. Zakrzewski, “Compression as a tool to detect Bose glass in a cold atomic gas,” *Phys. Rev. Lett.* **102**, 085301 (2009).
- [43] S. J. Thomson and F. Krüger, “Replica symmetry breaking in the Bose glass,” *EPL* **108**, 30002 (2014).
- [44] S. Morrison, A. Kantian, A. J. Daley, H. G. Katzgraber, M. Lewenstein, H. P. Büchler, and P. Zoller, “Physical replicas and the Bose glass in cold atomic gases,” *New J. Phys.* **10**, 073032 (2008).
- [45] W. S. Bakr, J. I. Gillen, A. Peng, S. Fölling, and M. Greiner, “A quantum gas microscope for detecting single atoms in a Hubbard-regime optical lattice,” *Nature (London)* **462**, 74 (2009).
- [46] R. Bai, S. Bandyopadhyay, S. Pal, K. Suthar, and D. Angom, “Bosonic quantum Hall states in single-layer two-dimensional optical lattices,” *Phys. Rev. A* **98**, 023606 (2018).
- [47] R. Graham and A. Pelster, “Order via nonlinearity in randomly confined Bose gases,” *Int. J. Bifurc. Chaos* **19**, 2745 (2009).
- [48] T. Khellil and A. Pelster, “Hartree-Fock mean-field theory for trapped dirty bosons,” *J. Stat. Mech.* **2016**, 063301 (2016).
- [49] F. Gerbier, “Boson Mott insulators at finite temperatures,” *Phys. Rev. Lett.* **99**, 120405 (2007).
- [50] K.-K. Ng, “Thermal phase transitions of supersolids in the extended Bose-Hubbard model,” *Phys. Rev. B* **82**, 184505 (2010).
- [51] F. Lin, T. A. Maier, and V. W. Scarola, “Disordered supersolids in the extended Bose-Hubbard model,” *Sci. Rep.* **7**, 1 (2017).